mRNA localization in endothelial cells regulates blood vessel sprouting

Guilherme Costa[1], Nawseen Tarannum[1] and Shane P. Herbert[1,2,*]

[1]Faculty of Biology, Medicine and Health, The University of Manchester, Manchester, M13 9PT, UK

[2]Lead Contact

*Correspondence: shane.herbert@manchester.ac.uk (S.P.H.)

SUMMARY

The subcellular targeting of mRNAs is fundamental to the spatial regulation of gene expression. However, whether mRNA localization directs complex morphogenetic events underpinning tissue development remains unknown. Here we reveal that spatial modulation of transcripts defines a novel paradigm for directional control of tissue movement and morphogenesis. Focusing on angiogenesis as a morphogenetic model, we identify *RAB13* as a key vascular transcript targeted and locally translated at the leading edge of migrating endothelial cells. We define the 3'UTR "zipcode" driving *RAB13* targeting and use novel vascular-specific MS2-MCP RNA-labelling tools in zebrafish to uniquely reveal the precise spatiotemporal dynamics of RNA localization in migratory cell processes *in-vivo*. Moreover, mutation of the endogenous zebrafish *rab13* 3'UTR disrupts transcript localization and perturbs endothelial cell protrusion dynamics during angiogenesis. Hence, local mRNA targeting imparts key spatial information on developing tissues, suggesting broad roles in the directional control of tissue formation in health and disease.

INTRODUCTION

mRNA localization is a well-established and crucial determinant of cell polarity (Buxbaum et al., 2015). Subcellular distribution of transcripts restricts translation to particular locations within the cell and it has been suggested to facilitate local protein activity. This mode of spatial control of gene expression contributes to rapid and localized cellular responses with implications in development and disease (Chin and Lecuyer, 2017). Although many of the protein-mediated mechanisms that regulate cell migration are well understood, only a handful of studies have delved thoroughly into the implications of mRNA localization in cell movement (Kislauskis et al., 1994, 1997; Liao et al., 2011; Schedlich et al., 1997; Shestakova et al., 2001; Wang et al., 2017). Much effort has been dedicated to understanding *β-ACTIN* mRNA localization, a transcript typically enriched at the leading front of motile cells and whose subcellular distribution is mediated by a short element in its 3' UTR (Kislauskis et al., 1994, 1997; Liao et al., 2011; Park et al., 2014; Schedlich et al., 1997; Shestakova et al., 2001; Wang et al., 2017). Nevertheless, these findings have been limited to *in vitro or ex vivo* observations, as live visualization of mRNA distribution in complex organisms is challenging. Moreover, despite the recent application of methods developed to image RNA localization in yeast cells (Bertrand et al., 1998) being applied to visualize RNAs in zebrafish embryonic cells (Campbell et al., 2015), the dynamic subcellular localization of mRNAs *in-vivo* and function in coordinating complex morphogenetic events, such as angiogenesis, remains unexplored.

Most new blood vessels emerge through angiogenic sprouting, an intricate morphogenetic

process that entails the coordinated migration of endothelial cells branching from parental vessels (Herbert and Stainier, 2011). Critical guidance cues such as the Vascular Endothelial Growth Factor (VEGF) secreted by the surrounding tissues regulate the molecular and cellular responses of endothelial cells triggered during angiogenesis (Gerhardt et al., 2003; Ruhrberg et al., 2002). Similar to other collective cell migration systems (Mayor and Etienne-Manneville, 2016), endothelial cells within sprouting vessels are hierarchically organized into leader tip cells and follower stalk cells (Arima et al., 2011; Gerhardt et al., 2003). Tip cells are highly polarized, presenting a leading edge that extends filopodia-containing protrusions and interacts with the extracellular matrix, whilst their rear engages in cell-to-cell contacts with stalk cells (Bentley et al., 2014; Gerhardt et al., 2003). Asymmetric distribution of cytoplasmic components contributes to dynamic membrane remodeling phenomena that are constrained to the cell-leading front during migration (Krause and Gautreau, 2014). Moreover, this inherent asymmetry is crucial for the maintenance of cell hierarchies following tip cell division during blood vessel growth (Costa et al., 2016). Whether the subcellular distribution of mRNAs is part of the polarity-defining asymmetry that controls endothelial cell migration during angiogenesis is unknown.

RAB13 belongs to the large RAB family of proteins, small GTPases that act as molecular switches controlling intracellular vesicle trafficking in many biological processes (Bhuin and Roy, 2014). Firstly reported as a key modulator of tight junction maintenance in epithelial cells (Marzesco et al., 2002; Zahraoui et al., 1994), RAB13 participates in cytoskeletal remodeling through the activity of its effector protein MICAL-L2 (Sakane et al., 2012; Sakane et al., 2013). RAB13 changes the conformational structure of MICAL-L2, which in turn interacts with the actin-binding proteins of the Filamin family and ultimately leads to membrane rearrangements at the leading edge of migrating cells (Sakane et al., 2013). More recently, Ioannou et al. (2015) have elegantly shown with biosensor tools that the RAB13 guanine exchange factor (GEF) DENND2B switches RAB13 into its active form at the leading edge of invasive tumor cells. The role of RAB13 in migration has also been demonstrated in VEGF-guided motility of endothelial cells. In this context, RAB13-mediated trafficking delivers the GEF Syx to the cell front, where together with its substrate RhoA modulates endothelial cell migration (Wu et al., 2011). Although RAB13 mRNA has been previously identified in protrusions formed at the front of migrating fibroblasts and tumor cells (Jakobsen et al., 2013; Mardakheh et al., 2015; Mili et al., 2008), the *in-vivo* morphogenetic function of the intracellular targeting of *RAB13* mRNA (or indeed any other mRNA) is currently unknown.

Here, we sought to investigate whether subcellular targeting of mRNAs defines a novel paradigm for the dynamic control of tissue morphogenesis. Using angiogenesis as a model morphogenetic system, we performed a transcriptome-wide screen of mRNAs enriched in protrusions formed at the leading edge of endothelial cells and identified *RAB13* as one of the most abundant transcripts.

Visualization of *RAB13* mRNA unveiled a notable polarization towards the migratory front of angiogenic endothelial cells, as well as local translation. Moreover, using novel vascular-specific reporter transgenics and live imaging in zebrafish, we show for the first time the dynamic localization of targeted mRNAs to migratory protrusions *in vivo*. Finally, to assess the functional role of localized *rab13* transcripts in this context, we generated a 3' UTR deletion mutant zebrafish strain and report abnormal protrusion formation and migratory dynamics of sprouting embryonic vessels. Hence, we reveal for the first time that polarized targeting of mRNAs, and not just their expression, modulates directional motile cell behavior and dictates tissue morphogenesis in vertebrate organisms.

RESULTS

The endothelial cell transcriptome is asymmetrically distributed during migration.

Extensive research over the last two decades has established the subcellular localization of mRNA as a key determinant in the spatial regulation of gene expression (Chin and Lecuyer, 2017). To start investigating the implications of this biological mechanism in endothelial cell migration and angiogenesis, we carried out a series of assays culturing Human Umbilical Vein Endothelial Cells (HUVECs) in modified Boyden chambers (Boyden, 1962) (hereafter referred as Transwells). This experimental setup allows the leading edge of migrating cells to extend protrusions through porous membranes separating two media-containing chambers and has been widely used to isolate compartmentalized mRNAs from diverse cell types (Jakobsen et al., 2013; Mili et al., 2008; Stuart et al., 2008; Zappulo et al., 2017). Thus, HUVECs were cultured for 2 hours in the upper chambers of Transwells containing 3µm pore membranes, in low serum conditions. Subsequently, VEGF-A was added to the lower Transwell chamber to promote cell migration through the membranes (Lee et al., 2002) during the following hour (**Figure 1A**). The short culture periods permit the formation of protrusions during the initial stages of migration into the lower chambers whilst the cell bodies remain in the upper chamber. In order to investigate whether HUVECs preferentially localize transcripts to their leading edge, RNA was extracted from cell bodies and protrusions to perform a high-throughput screen (RNA-seq). In these studies, we identified a set of 320 mRNAs enriched in HUVEC protrusions (fold change >1.6) when compared to mRNAs present in the cell body fraction (**Figure 1B**). Many of the mRNAs we detected in protrusions encode proteins that regulate cell motility and have also been identified as transcripts preferentially localized to the leading edge of highly migratory cells (**Table S1A**). One of these transcripts encodes *RAB13*, a small GTPase associated with cell membrane dynamics underlying cell migration (Ioannou et al., 2015; Sakane et al., 2013), which was amongst the transcripts with the highest levels of enrichment in HUVECs (**Figures 1B** and **1C**). In

contrast, the classical protrusion-related *β-ACTIN* mRNA presented a rather modest enrichment and transcripts encoding the membrane-bound VEGFR2 were more abundant in cell bodies (**Figures 1B** and **1C**). Interestingly, we noted that no other transcripts encoding RAB proteins expressed in HUVECs were enriched in protrusions (**Figure 1B; Table S1B**). These distinctive aspects of *RAB13* prompted us to study it as a model for localized mRNA function in migrating endothelial cells.

***RAB13* mRNA is localized at the distal end of tip cells during angiogenesis.**

To characterize in detail the subcellular distribution of *RAB13* transcripts, we performed single molecule fluorescent *in situ* hybridization (smFISH) using HUVECs maintained in different culture contexts. Firstly, sparse cells cultured in 2D surfaces were fixed and hybridized with probes recognizing *RAB13* mRNA in combination with probes detecting the control transcript *GAPDH* (**Figure 1D and S1A**). The transcript distribution was subsequently quantified using an analytical method developed by Park et al. (2012) for cell cultures in 2D, which measures the displacement of the center of mRNA distribution from the cell center in the form of a Polarization Index (PI). These experiments showed a striking asymmetric distribution of *RAB13* mRNA (PI 0.67) when compared *GAPDH* mRNA (PI 0.24) in a randomly sampled population of individual HUVECs (**Figure 1E**). Next, to study transcript localization in the context of collective endothelial cell migration, we carried out smFISH using scratch wound assays to compare mRNA distribution in leader cells with follower cells. To do so, HUVECs were cultured to confluence and a wound was induced to promote oriented migration towards the cleared space. Leader cells present at the wound edge showed an increased *RAB13* mRNA polarization level (PI 0.76) than cells follower cells located in confluent areas (PI 0.50) (**Figures S1C-S1G)**. Interestingly, the mean number of smFISH spots detected in leader cells (70 spots) was significantly higher than in follower cells (42 spots) indicating that leader cells upregulate *RAB13* (**Figure S1H)**.

Although the scratch wound assay generates leader and follower cells and confers directionality to collectively migrating cells, it does not recapitulate many of the complex processes that take place in 3D physiological environments during angiogenesis. Hence, to visualize and characterize the subcellular distribution of *RAB13* mRNA in cells at the leading front of growing blood vessels, we opted to perform *in vitro* angiogenesis assays. Microbeads coated with HUVECs were cultured in a fibrin matrix covered by a monolayer of fibroblasts to promote the chemotactic angiogenic sprouting (Nakatsu and Hughes, 2008). Remarkably, the distal-most region of tip leader cells within sprouts showed a strong accumulation of *RAB13* mRNA (**Figure 1F** and **S1B**). Given that assessing transcript PIs in 3D proved technically challenging, we measured the relative distance between the center of mRNA distribution and the cell nucleus to compare the distribution of *RAB13* and *GAPDH* transcripts. Applying this method, we observed that *RAB13* mRNA displayed a higher distal

distribution (relative distance 0.54) than *GAPDH* mRNA (relative distance 0.33) (**Figure 1G**). Altogether, these observations not only validate the RNA-seq data but also led us to further investigate the implications of *RAB13* mRNA localization in angiogenesis.

RAB13 is translated at the leading edge of endothelial cells during migration

To verify whether translation of localized mRNAs can take place in protrusions formed at the leading edge of endothelial cells, HUVECs were cultured in Transwells as described above and Puromycin was briefly added the to lower chambers at the end of the assay. Puromycin incorporates nascent peptide chains and labels newly translated proteins that can be recognised by immuno-detection. HUVEC protrusions containing puromycinilated proteins were found in the lower side of Transwells membranes but not in those cultured without Puromycin or those co-treated with the translation inhibitor Anisomycin (**Figure S2A**). To exclude potential puromycinilation of proteins synthesized by cell bodies and transported into protrusions, the former were removed prior to a short incubation with or without Puromycin or with a combination of Puromycin and Anisomycin (**Figure 2A**). Likewise, protrusions containing puromycinilated proteins were detected in cell body-free Transwell membranes exposed to Puromycin, but not when also treated with Anisomycin (**Figure 2B**). Our observations indicated HUVEC protrusions contain active translational machinery that synthesizes proteins independently of cell bodies. However the puromycylation of newly synthesized proteins can be further used in combination with antibody-based proximity ligation assays (Puro-PLA) to detect local translation of proteins of interest (tom Dieck et al., 2015). To test whether RAB13 is locally translated, Puro-PLA experiments were performed with HUVEC protrusions segregated from cell bodies. Using antibodies targeting RAB13 and Puromycin, we observed higher levels of PLA signal (0.01 puncta/μm^2) in protrusions exposed to Puromycin than those in Puromycin-free control cultures (0.002 puncta/μm^2) (**Figures 2C** and **2D**) or in the absence of antibodies (0.001 puncta/μm^2) (**Figure S2B and S2C**). Upon treatment with Anisomycin, the PLA signal was significantly reduced (0.004 puncta/μm^2) (**Figures 2C** and **2D**). In summary, these results demonstrate that *RAB13* and likely other mRNAs are spatially targeted to and actively translated at the leading of migratory endothelial cells.

Identification of *RAB13* mRNA sequences that localize transcripts *in vitro* and *in vivo*.

Localization elements mediating the subcellular distribution of mRNAs are commonly found within 3' UTRs (Andreassi et al., 2010; Aschrafi et al., 2010; Brittis et al., 2002; Kislauskis et al., 1994; Mili et al., 2008; Wu et al., 2005). In fact, the 3' UTR of the mouse *RAB13* orthologue has been shown to localize transcripts to protrusion of mouse fibroblasts (Mili et al., 2008) using the MS2 system developed by the Singer lab (Bertrand et al., 1998), but any specific "zipcode" sequence responsible

is unknown. With the MS2 modular tool, RNA regions of interest are tagged with repeats of the bacteriophage-derived MS2 hairpin, a high affinity sequence for the MS2 capping protein (MCP). Subsequently, MCP fused to the green fluorescent protein (MCP-GFP) is co-expressed in the cell of interest with MS2 tagged RNA to investigate transcript behavior in living cells. To begin defining the *RAB13* 3' UTR localization element, we cloned the 3' UTR downstream of a cassette containing 24 MS2 hairpins and co-transfected it with a nuclear from of MCP-GFP(nls) into endothelial cells. Whilst in control transfections MCP-GFPnls expression was restricted to the nucleus, cells transfected with MS2-tagged *RAB13* 3' UTR formed protrusions with local accumulation of MCP-GFPnls (**Figure 3A**). Moreover, deleting fragments within the *RAB13* 3' UTR revealed that minimal region between nucleotide positions 90-282(nt) within *RAB13* 3' UTR was sufficient and necessary to localize MCP-GFPnls to endothelial cell protrusions (**Figures 3B** and **S3A**). Next, to examine whether this region is indeed responsible for the subcellular distribution of endogenous transcripts, we used CRISPr/Cas9 tools to excise it from the genomic *RAB13* locus of HUVECs (**Figure S3B)**. In contrast to control cells that maintained the characteristic localization of *RAB13* mRNA, CRISPr-edited HUVECs showed a remarkable reduction in the accumulation of *RAB13* transcripts in protrusions (**Figures 3C** and **S3C**) and decreased *mRNA* polarization levels (**Figures 3D**). Hence, we define a 192 nt sequence that is necessary and sufficient to drive targeting of mRNAs to the leading edge of migrating cells.

The zebrafish embryo is a powerful and well-established tool to study angiogenesis and many fluorescent transgenic strains have been generated to visualize the development of blood vessels in living animals (Hogan and Schulte-Merker, 2017). Hence, to further understand the *in-vivo* implications of asymmetric mRNA distributions in tissue morphogenesis we set out to study whether the zebrafish *RAB13* 3' UTR orthologue also localizes transcripts in endothelial cells during embryonic vascular development. To visualize the localization of *rab13* mRNA *in vivo* during angiogenesis, we generated a vascular-specific MCP-GFPnls transgenic zebrafish strain *Tg(fli1ep:*MCP-GFPnls*)* (**Figure S3D**). Single cell stage transgenic embryos were injected with a construct containing the zebrafish *rab13* 3' UTR downstream of 24 MS2 hairpins and the membrane-targeted fluorescent protein Lyn-mCherry (**Figure S3E**). One day later, embryos with mosaic expression of Lyn-mCherry were examined using confocal imaging. We focused on intersegmental vessels (ISVs), a well-characterized vessel bed that sprouts from the embryonic dorsal aorta (Isogai et al., 2003). In these embryos, Lyn-mCherry-expressing endothelial cells within ISVs displayed a striking accumulation of MCP-GFPnls in distal protrusions that extended towards the dorsal side of the embryo (**Figure 3E; Movie S1**). The distribution of MCP-GFPnls in endothelial cell protrusions was extremely dynamic, reflecting the rapid remodeling of the cell membrane during migration. Importantly, this non-nuclear localization of MCP-GFPnls demonstrates that the *rab13* 3' UTR also

localizes transcripts to the leading edge of angiogenic endothelial cells *in vivo.* Moreover, our data show, for the first time, tissue-specific visualization of mRNA localization within a living vertebrate organism.

The asymmetrical distribution of *rab13* mRNA fine-tunes angiogenic sprouting

Following our *in vivo* observations, we sought to investigate the role of *rab13* mRNA localization during endothelial cell migration in zebrafish embryos. The use of genetic tools to delete 3' UTRs has been a strategy successfully used in studying the implications of subcellular transcript localization in neurons (An et al., 2008; Miller et al., 2002). However, *in vivo* functional roles for localized mRNAs in tissue migration and vertebrate morphogenesis have not been explored. Thus, we applied CRISPr/Cas9 technology to delete a 482nt fragment of the *rab13* 3' UTR (Δ482 *rab13* 3' UTR hereafter) that we predicted to entail the mRNA targeting sequence (**Figure S4A**). This deletion was generated in the zebrafish *Tg(flk1:*EGFP*)^{s843}* transgenic background to facilitate the visualization of developing blood vessels (Jin et al., 2005). Breeding heterozygous animals generated progeny with expected Mendelian frequencies (**Figures S4B** and **S4C)** and with no significant changes in the relative levels of *rab13* mRNA at 22-26 hours post fertilization (hpf) (**Figure S4D)**. In order to confirm that disrupting the 3' UTR of *rab13* results in transcript mislocalization, 24 hpf embryos obtained from incrossed heterozygous Δ482 *rab13* 3' UTR zebrafish were dissociated and cultured for 18 hours and analyzed with smFISH assays. The polarization levels of *rab13* mRNA were significantly reduced in homozygous cells (PI 0.35) when compared to wild type counterparts derived from sibling embryos (PI 0.53) (**Figures 4A** and **4B),** whilst heterozygous cells displayed intermediate levels (PI 0.43) (**Figure 4B)**. Having demonstrated that the 3' UTR of zebrafish *rab13* mediates endogenous transcript distribution, we next assessed whether mislocalizing *rab13* affects angiogenic sprouting in zebrafish embryos. Thus, time-lapse confocal microscopy was used to image developing ISVs in sibling embryos generated from Δ482 *rab13* 3' UTR heterozygous *Tg(flk1:*EGFP*)^{s843}* fish. Whilst the position at which growing ISVs will turn and fuse with adjacent ISVs to form the dorsal longitudinal anastomotic vessel (DLAV) was unchanged in any genotype (**Figure S4E)**, homozygous Δ482 *rab13* 3' UTR embryos showed a higher frequency (66%) of ISVs containing transient vessel branches emerging from the main ISV sprout than heterozygous (45%) and wild type (33%) counterparts (**Figures 4C** and **S4F; Movie S2)**. Furthermore, we observed that branching typically occurred at the leading front of sprouting vessels in two main embryonic regions: 1) close to the dorsal side of the embryo, immediately before the ISVs formed of the DLAV and 2) close to the horizontal myoseptum (HM) at the earlier stages of the ISV spouting process (**Figure 4D)**. These types of branching may reflect different stages of decision-making processes that endothelial cells face during guided migration to correctly form blood vessels. Indeed, transient vessel

branching at the dorsal side of the embryo before formation of the DLAV was a common feature of WT branching. However, ISVs presenting transient mis-guided branches close to HM were uncommon in wild types and were detected with much higher frequencies in homozygous Δ482 *rab13* 3' UTR embryos (64%) than in heterozygous (19%) and wild type siblings (13%) (**Figure 4E)**. Hence, intracellular targeting of *rab13* mRNA (and not expression of the transcript *per se*) provides critical positional information that directs the normal guidance of developing vessels. As such, we reveal for the first time that the correct subcellular distribution of mRNAs can coordinate vertebrate tissue morphogenesis.

DISCUSSION

The polarization of cellular components is a key cellular feature during migration. Polarized cells actively remodel their microfilament network at their leading edge resulting in an array of rapid and dynamic rearrangements of the plasma membrane. Thus, the polarized formation of membrane protrusions at the leading edge mediates migration guidance in response to microenvironmental cues (Krause and Gautreau, 2014). During angiogenesis, endothelial cells collectively polarize and migrate to form new blood vessels. In addition, we have recently shown that tip cells at the leading front of sprouting vessels divide asymmetrically to ensure their critical polarized properties are rapidly re-established following division (Costa et al., 2016). Here, we unveil that endothelial migratory polarity is unexpectedly driven by the asymmetric distribution of mRNAs, and that such subcellular localization of *RAB13* transcripts coordinates protrusion formation during blood vessels morphogenesis.

In groups of endothelial cells undergoing collective cell migration, leader cells not only show higher polarization of *RAB13* mRNA but also contain increased *RAB13* transcript levels. Moreover, although motile HUVECs express many of the genes encoding RAB proteins, only *RAB13* transcripts are highly enriched in protrusions. This not only strongly suggests a transcript-specific role for the asymmetric distribution of *RAB13* mRNA in the control of angiogenesis but also offers an excellent model transcript to study mRNA localization in tissue morphogenesis *in vivo*. Although targeting of *RAB13* mRNA to the leading edge has been previously reported in other cell types *in vitro* (Jakobsen et al., 2013; Mili et al., 2008; Zappulo et al., 2017) and is known to require the 3'UTR (Mili et al., 2008), the targeting motifs responsible for this localization of *RAB13*, its global importance for driving cell migration and physiological function in complex morphogenetic processes *in vivo* had yet to be addressed. Here we have defined the specific targeting region driving *RAB13* targeting and demonstrated that equivalent regions of the zebrafish mRNA drive localization of transcripts to

protrusions formed at the leading edge of migrating cells *in vivo*. Furthermore, the deletion of this region induces the formation of extra branching at the leading front of zebrafish ISVs at early stages of embryonic vessel sprouting, revealing that the 3' UTR-mediated localization of *RAB13* mRNA (but not its expression *per se*) is involved in cell path finding. It is tempting to speculate that the accumulation of *RAB13* mRNA in the correct subcellular location normally allows the persistence of protrusions along the correct migration path, in detriment of alternative protrusion formation at the leading front of the vessel. Moreover, the transport of *RAB13* transcripts in fibroblast protrusions has been partly attributed to the adenomatous polyposis coli (APC) (Mili et al., 2008; Wang et al., 2017), a tumor suppressor protein found at the leading front of endothelial cells (Harris and Nelson, 2010). Hence, it will be key to determine whether APC interacts directly with the *RAB13* 3' UTR 192 nt targeting sequence or indirectly through other RNA-binding proteins and if similar cell guidance phenotypes are observed upon loss of APC-mediated transport *in vivo.*

The proportion of protrusion-enriched mRNAs that undergo translation has been reported with disparity in distinct cell types. While Mardakheh et al. (2015) suggested that most mRNAs enriched in tumor cell protrusions are in fact translationally repressed, Zappulo et al. (2017) reported that a great part of the transcripts localized to neuronal processes undergo translation. Using an *in-situ* visualization approach, we verified that *RAB13* mRNA is actively translated in endothelial protrusions independently of the cell body, indicating that the localization of the transcript provides newly synthesized RAB13 to the leading edge the cell. The synthesis of RAB proteins in the cytosol has been proposed to contribute to a pool of newly translated RAB proteins different from pre-existing ones that display distinct interacting partners (Seabra et al., 2002). RAB escorting proteins (REPs) interact with newly synthesized RAB proteins in the cytosol to promote its prenylation and consequently, association with vesicular membranes (Shen and Seabra, 1996). On the other hand, pre-existing RAB proteins bound to GDP are displaced from membranes by the GDP dissociation inhibitor (GDIs) and targeted for recycling (Pfeffer et al., 1995). The ability of REPs and GDIs to differentially regulate the two pools may result in distinct biological outcomes. It is plausible that newly translated *RAB13* in its unmodified form is rapidly available to be deposited in membrane vesicles and exert its molecular control of microfilament rearrangement at leading edge of migrating cells. Alternatively, localized translation could simply increase the local concentration of RAB13 presented to its activator GEFs in protrusions. Hence, in our angiogenesis studies, the absence of polarized *rab13* transcripts in zebrafish embryos would reduce local amounts of newly synthesized protein, resulting in abnormal protrusion formation during blood vessel sprouting.

In summary, the studies presented here provide novel insights into the involvement of subcellular mRNA localization in complex morphogenetic events *in vivo* and define a new paradigm for the molecular control of directional blood vessel growth and vertebrate tissue morphogenesis.

AUTHOR CONTRIBUTIONS

Conceptualization, G.C. and S.P.H.; Methodology, G.C.; Formal Analysis, G.C.; Investigation, G.C. and N.T.; Writing – original draft, G.C.; Writing – review and editing, S.P.H.; Supervision, G.C. and S.P.H.; Funding acquisition, S.P.H.

ACKNOWLEDGMENTS

We wish to thank members of the Biological Services, Genomic Technologies and Bioimaging Facilities at the FBMH, University of Manchester, for technical support. We are grateful to E. Schuman and S. tom Dieck at the MPI for Brain Research for help and guidance setting up the Puro-PLA assays. We also thank N. Papalopulu and members of for her research group at the FBMH, University of Manchester, for critical feedback and for providing reagents and materials. This work was funded by the Wellcome Trust (095718/Z/11/Z to S.P.H.), Wellcome Institutional Strategic Support Fund (7064646 to G.C.) and the British Heart Foundation (PG/16/2/31863 to S.P.H.).

DECLARATION OF INTERESTS

The authors declare no competing interests

METHODS

Zebrafish husbandry

Zebrafish were maintained and bred according to standard conditions. Experimental procedures were approved by the University of Manchester Ethical Review Board and performed according to UK Home Office regulations.

Embryo micro-injections and generation of zebrafish strains

To generate the transgenic zebrafish strain *Tg(fli1ep:*MCP-GFPnls*)* using Tol2 transposon transgenesis, 32 pg of Cerulean-H2B:bas*fli1ep*:MCP-GFPnls Tol2-based plasmid was co-injected with 32 pg Tol2 mRNA into one-cell stage AB zebrafish embryos. The next day, embryos with mosaic GFP expression were selected, raised into adulthood and then outbred to AB zebrafish to identify founders with germ-line transmission of the transgene. Adult *Tg(fli1ep:*MCP-GFPnls) were inbred and one-cell stage embryos were co-injected with 32 pg of Cerulean-H2B:bas*fli1ep:*Lyn-mCherry-24xMS2-*rab13*-3'UTR Tol2-based plasmid and 32 pg Tol2 mRNA for mosaic expression analysis.

The mutant Δ482 *rab13* 3' UTR strain was generated with CRISPr/Cas9 tools. One-cell stage *Tg(flk1:*EGFP*)*^{s843} embryos were injected with 150 pg of each *in vitro* transcribed gRNA and co-injected with 150 pg Cas9 NLS nuclease (New England Biolabs). Embryos were raised into adulthood and outbred to AB zebrafish to identify founders with germ-line transmission of a mutant *rab13* 3' UTR.

gRNA generation and *in vitro* transcription

The online CRISPRscan tool (Moreno-Mateos et al., 2015) was used to design gRNAs targeting the zebrafish 3' UTR region in the *rab13* locus (**Table S2**). Next, 0.3 µM oligonucleotides comprising the target sequences (flanked by the T7 promoter and the Tail annealing sequence) were mixed with 0.45 µM Tail primer (**Table S2**) and PCR amplified with Platinum Pfx DNA polymerase (Thermo Fisher) in a T100 thermal cycler (BioRad). The following cycling conditions were used: 1 cycle of initial denaturation at 94°C for 10 minutes, 30 cycles of denaturation at 94°C for 30 seconds, annealing at 45°C for 30 seconds, extension at 68°C for 30 seconds, and a final extension cycle at 68°C for7 minutes. Subsequently, 200 ng of PCR amplified templates were used to transcribe gRNAs using a MEGAshortscript T7 Transcription Kit (Thermo Fisher), following the manufacturer's recommendations.

To synthesize Tol2 mRNA, 1 µg NotI-linearized pCS2-TP plasmid was transcribed using a SP6 mMESSAGE mMACHINE kit (Thermo Fisher) according to manufacturer's protocol.

Embryo genotyping

Genomic DNA was extracted incubating either whole embryos or embryo heads in lysis buffer (10 mM Tris HCl pH8, 1 mM EDTA, 80 mM KCl, 0.3% NP40, 0.3% Tween) containing 0.5 µg/µl Proteinase K (Promega) at 55°C for 1-2 hours, followed by a denaturation step at 95°C for 15 minutes in a T100 thermal cycler. Genotyping PCR was performed using 2 µl genomic DNA, 0.4 µM zebrafish genotyping primers (**Figure S4A**, **Table S2**) and 1 x MyTaq Red DNA Polymerase (Bioline) according to the manufacturer's protocol in a T100 thermal cycler. PCR reactions were resolved in 1 % agarose (Bioline) gels containing 0.5 µg/ml Ethidium Bromide (Sigma) for analysis.

Cell culture

Trunks of 26-28 hpf embryos were incubated in Trypsin-EDTA solution (Sigma) at 28°C for 15 minutes. Trypsinization was quenched with complete L-15 medium (Sigma) containing 10 % Fetal Bovine Serum (FBS, Sigma) and 10 U/ml-100µg/ml Penicillin-Streptomycin (Sigma). Cells were pelleted at 2000 rpm for 5 minutes at room temperature (RT), resuspended in complete L-15 medium, plated on Laminin-coated (Sigma) coverslips in 24 well plates and maintained at 28°C for 18 hours. HUVECs (PromoCell) were cultured in complete ECGM2 (PromoCell) in gelatin-coated (Millipore) dishes. Human Pulmonary Fibroblasts (PromoCell) were cultured in M199 (Thermo Fisher) containing 10 % FBS, 50 µg/ml Gentamycin (Sigma) and 50 ng/ml Amphotericin (Sigma). Brain endothelial (bEnd.3) were cultured in DMEM (Sigma) supplemented with 10 % FBS, 10 ng/ml Recombinant Human VEGF-A (PeproTech) and 10 U/ml-100µg/ml Penicillin-Streptomycin. All cell types were incubated in standard culture conditions, with 5% CO_2 at 37°C.

CRISPr/Cas9 cell editing and cell transfections

To edit RAB13 locus, HUVECs were transfected with Alt-R CRISPr/Cas9 ribonucleoprotein complexes (Integrated DNA Technologies) targeting the 90-182nt localization element within the 3' UTR. Briefly, each sequence-specific crRNA (**Table S2**) was mixed with tracrRNA at 1:1 50 µM, incubated at 95°C for 5 minutes in a T100 thermal cycler and allowed to cool to RT for 60 minutes. Next, 12 µM each crRNA:tracrRNA (gRNA) was incubated with 20 µM Alt-R Cas9 nuclease in PBS (Sigma) at RT for 20 minutes to form ribonucleoprotein complexes and mixed with $500x10^3$ HUVECs. Additionally, 2 µg pmaxGFP Vector (Lonza) was included in the HUVEC-ribonucleoprotein mix to identify transfected cells. Transfections were performed in a Nucleofector 2b Device (Lonza), using a HUVEC Nucleofector kit (Lonza) according to manufacturer's instructions and the cells were further cultured for 72 hours. Afterwards, single GFP-expressing cells were isolated in a FACS Aria Fusion cell sorter (BD Biosciences) into gelatin-coated 96 well plates

to grow individual clones. Genomic DNA was extracted from expanded HUVEC clones and PCR-analyzed with sequence-specific primers (**Table S2**) as described for zebrafish embryo genotyping.
For *in vitro* MS2 experiments, bEnd.3 were transfected with pcDNA3-Lyn-mCherry, pCS2-MCP-GFPnls and different versions of pcDNA3-*HBB*-24XMS2SL-*RAB13* 3' UTR. Briefly, $100x10^3$ cells / well cultured in 6 well plates were transfected with 0.8 µg each plasmid DNA using Lipofectamin2000 following the manufacturer's protocol (Thermo Fisher) and analyzed 48 hours later.

Transwell assays and cell body / protrusion fractionation

Transwell experiments to segregate cell bodies and protrusions were performed as described elsewhere (Mili et al., 2008), with the following modifications: $1.5x10^6$ HUVECs were cultured for 2 hours in 24 mm Transwells (Costar), containing 3µm-pore polycarbonate membranes, in M199 (Thermo Fisher) supplemented with 1 % FBS. Subsequently, 25ng/ml VEGF-A was added to the lower chambers to promote cell migration over the next hour. While only 1 Transwell was used for the cell body fraction, 2 Transwells were used to harvest HUVEC protrusions.

RNA isolation, qPCR and RNA-seq

Embryo and cell-derived RNA was isolated using a RNAqueous-Micro Kit (Thermo Fisher) according to the manufacturer's protocol. For gene expression analysis, cDNA was synthesized with a High-Capacity RNA-to-cDNA kit (Thermo Fisher) following the manufacturer's protocol.
qPCR experiments were performed with 1-2 µl cDNA, 0.25 µM gene-specific primers (**Table S2**) and 1 x Power SYBR Green Master Mix (Thermo Fisher) in a StepOne Real-Time PCR System (Applied Biosystems). Either human or zebrafish *GAPDH* expression was used to normalize gene expression levels and the relative mRNA levels were analyzed with the $2^{-\Delta\Delta CT}$ method.
For RNA-seq, quality and integrity of RNA samples obtained from HUVEC cell bodies and protrusions were assessed using a 2200 TapeStation (Agilent Technologies). Next, RNA-seq libraries were generated using the TruSeq Stranded mRNA assay (Illumina) according to the manufacturer's protocol. Adapter indices were used to multiplex libraries, which were pooled prior to cluster generation using a cBot instrument. The loaded flow-cell was then paired-end sequenced (76 + 76 cycles, plus indices) on an Illumina HiSeq4000 instrument. Finally, the output data was demultiplexed (allowing one mismatch) and BCL-to-Fastq conversion performed using Illumina's bcl2fastq software, version 2.17.1.14

Fibrin sprout assay and scratch wound assay

Fibrin sprout assays were performed as previously described by Nakatsu and Hughes (2008) in HUVEC and HPF co-cultures. HUVECs cultured on gelatin coated coverslips were grown to confluence and used in scratch wound assays as described elsewhere (Liang et al., 2007).

smFISH

Zebrafish cells, HUVECs cultured in sparse conditions, fibrin sprouts and scratch wound assays were fixed in methanol free 4 % formaldehyde (Thermo Fisher) and used in smFISH assays. Stellaris smFISH probes (Biosearch Technologies) targeting human *RAB13*, human *GAPDH* and zebrafish *RAB13* transcripts were purchased from Biosearch Technologies with Q570 and Q670 fluorophore modifications and used according to the manufacturer's manual.

Puro-PLA and immunofluorescence

Cell bodies of HUVECs cultured in Transwells were scraped and remaining protrusions were exposed to 3 µM Puromycin (Sigma) added to lower chambers for 6 minutes. In translation inhibition experiments, 40 µM Anisomycin (Sigma) was added to the lower Transwell chamber 30 minutes before cell body removal and 6 minutes after cell body removal together with 3 µM Puromycin. Subsequently, HUVEC protrusions grown in Transwell membranes were fixed in methanol free 4 % formaldehyde, removed from the Transwell inserts and used in Puro-PLA experiments as described elsewhere (tom Dieck et al., 2015) or immunofluorescence assays, using antibodies to detect RAB13 (Millipore) and Puromycin (Kerafast). Following the Puro-PLA protocol, Transwell membranes were incubated for 20 minutes with 1:40 Alexa Fluor 488 Phalloidin (Thermo Fisher) in PBS, washed in Duolink wash buffer B (Sigma) and mounted on microscope slides with Duolink *In Situ* Mounting Medium containing DAPI (Sigma).

For immunofluorescence experiments, Transwell membranes were permeabilized in PBS containing 0.5% Triton-X100 (Sigma) and 4 % goat serum (Sigma) for 15 minutes, and blocked with 4 % goat serum in PBS at 4°C overnight. Next, membranes were incubated with 1:3500 Puromycin in blocking buffer at RT for 1 hour, washed in PBS and incubated with a goat anti-mouse AlexaFluor 568 antibody (Thermo Fisher) at RT for 1 hour. Membranes were incubated with 1:40 Alexa Fluor 488 Phalloidin in PBS at RT for 20 minutes, washed in PBS and mounted on microscope slides with Vectashield antifade mounting medium containing DAPI (Vector Laboratories).

Plasmid construction

The pCS2-MCP-GFPnls plasmid used in *in vitro* MS2-system assays was generated excising a MCP-GFPnls fragment with SpeI and KpnI from pMS2-GFP, a gift from Robert Singer (Addgene plasmid # 27121) (Fusco et al., 2003), and subcloning it into a pCS2+ vector using the XbaI and KpnI sites.

To construct the Cerulean-H2B:*basfli1ep:*MCP-GFPnls Tol2-based plasmid for *in vivo* studies, MCP-GFPnls was amplified from pMS2-GFP with sequence 0.3 µM specific primers (**Table S2**) and Platinum Pfx DNA polymerase in a T100 thermal cycler. Subsequently, the PCR product was cloned into a pDONR221 P3-P2 using Gateway Technology (Thermo Fisher) according to manufacturer's manual. The final Tol2-based construct was assembled into the pTol2Dest(R1R2) (Addgene plasmid # 73484) (Villefranc et al., 2007) using Gateway 3-fragment recombination with pE(L1L4)Cerulean-H2B in the first position, pE(R4R3)*basfli1ep* (De Bock et al., 2013) in the second position and pE(L3L2)MCP-GFPnls in the third position.

For *in vitro* MS2-system experiments, the 3' UTR of human *RAB13* was PCR amplified with 0.3 µM sequence-specific primers (**Table S2**) using Platinum Pfx DNA polymerase in a T100 thermal cycler and the resulting PCR product was cloned using a Zero Blunt PCR cloning kit (Thermo Fisher), following the manufacturer's manual. Next, the human *HBB* gene was PCR amplified using 0.3 µM sequence-specific primers (**Table S2**) and Platinum Pfx DNA polymerase in a T100 thermal cycler and cloned into the NotI and BamHI sites of the pCR4-24XMS2SL-stable plasmid, a gift from Robert Singer (Addgene plasmid # 31865) (Bertrand et al., 1998). Subsequently, a multiple cloning site (MCS, **Table S2**) was introduced into the BglII and SpeI sites of pCR4-*HBB*-24XMS2SL and the recombinant *HBB*-24XMS2SL-MCS sequence was subcloned into the pcDNA3 mammalian expression vector (Thermo Fisher) using the NotI and XbaI sites. The full-length 482nt *RAB13* 3' UTR was then sub-cloned into pcDNA3-*HBB*-24XMS2SL-MCS using NheI and XhoI sites. Alternatively, truncated and deletion versions of *RAB13* 3' UTR were generated by PCR using 0.3 µM sequence-specific primers (**Table S2**) and Platinum Pfx DNA polymerase or using QuikChange II Site-Directed Mutagenesis kit (Agilent Technologies) following the manufacturer's instructions and introduced into the pcDNA3-*HBB*-24XMS2SL-MCS using the NheI and XhoI sites.

In order to generate the zebrafish MS2-system reporter construct, the 24XMS2SL cassette was firstly subcloned from pCR4-24XMS2SL-stable into a *kdrl:*Lyn-mCherry Tol2 based plasmid (Costa et al., 2016) using a BamHI site. Next, the zebrafish *rab13* 3' UTR was PCR amplified with 0.4 µM sequence specific primers (**Table S2**) and MyTaq Red DNA Polymerase from zebrafish genomic DNA in a T100 thermal cycler and then subcloned into the Tol2 *kdrl:*Lyn-mCherry-24XMS2SL plasmid using NheI and BglII sites. The resulting Lyn-mCherry-24XMS2SL-*rab13* 3' UTR recombinant sequence was amplified with 0.3 µM sequence-specific primers (**Table S2**) and Platinum Pfx DNA polymerase in a T100 thermal cycler and subcloned into a pDONR221 P3-P2

using Gateway Technology. Lastly, the final Tol2-based construct was assembled into the pTol2Dest(R1R2) using Gateway 3-fragment recombination with pE(L1L4)Cerulean-H2B in the first position, pE(R4R3)*basfli1ep* in the second position and Lyn-mCherry-24XMS2SL-*rab13* 3' UTR in the third position.

All plasmid maps and details are available upon request.

Microscopy

Confocal time-lapse imaging of zebrafish was carried out as previously described (Costa et al., 2016). Images of cultured cells and Transwell membranes were acquired on an Olympus IX83 inverted microscope using Lumencor LED excitation, either a 40x/ 1.00 UplanApo or a 60x/ 1.42 PlanApo objective and a Sedat QUAD (DAPI/FITC/TRITC/Cy5) filter set (Chroma 89000). The images were collected using a R6 (Qimaging) CCD camera with a Z optical spacing of 0.2 of 0.3 µm. Raw images were then deconvolved using the Huygens Pro software (SVI) and maximum intensity projections of these images were used for analysis.

Statistics

Statistical analysis of the data was carried out using GraphPad prism software, using parametric t-tests when the data were normally distributed or non-parametric Mann Whitney tests when the data did not pass normality tests.

REFERENCES

An, J.J., Gharami, K., Liao, G.Y., Woo, N.H., Lau, A.G., Vanevski, F., Torre, E.R., Jones, K.R., Feng, Y., Lu, B., *et al.* (2008). Distinct role of long 3' UTR BDNF mRNA in spine morphology and synaptic plasticity in hippocampal neurons. Cell *134*, 175-187.

Andreassi, C., Zimmermann, C., Mitter, R., Fusco, S., De Vita, S., Saiardi, A., and Riccio, A. (2010). An NGF-responsive element targets myo-inositol monophosphatase-1 mRNA to sympathetic neuron axons. Nat Neurosci *13*, 291-301.

Arima, S., Nishiyama, K., Ko, T., Arima, Y., Hakozaki, Y., Sugihara, K., Koseki, H., Uchijima, Y., Kurihara, Y., and Kurihara, H. (2011). Angiogenic morphogenesis driven by dynamic and heterogeneous collective endothelial cell movement. Development *138*, 4763-4776.

Aschrafi, A., Natera-Naranjo, O., Gioio, A.E., and Kaplan, B.B. (2010). Regulation of axonal trafficking of cytochrome c oxidase IV mRNA. Mol Cell Neurosci *43*, 422-430.

Bentley, K., Franco, C.A., Philippides, A., Blanco, R., Dierkes, M., Gebala, V., Stanchi, F., Jones, M., Aspalter, I.M., Cagna, G., *et al.* (2014). The role of differential VE-cadherin dynamics in cell rearrangement during angiogenesis. Nat Cell Biol *16*, 309-321.

Bertrand, E., Chartrand, P., Schaefer, M., Shenoy, S.M., Singer, R.H., and Long, R.M. (1998). Localization of ASH1 mRNA particles in living yeast. Mol Cell *2*, 437-445.

Bhuin, T., and Roy, J.K. (2014). Rab proteins: the key regulators of intracellular vesicle transport. Exp Cell Res *328*, 1-19.

Boyden, S. (1962). The chemotactic effect of mixtures of antibody and antigen on polymorphonuclear leucocytes. J Exp Med *115*, 453-466.

Brittis, P.A., Lu, Q., and Flanagan, J.G. (2002). Axonal protein synthesis provides a mechanism for localized regulation at an intermediate target. Cell *110*, 223-235.

Buxbaum, A.R., Haimovich, G., and Singer, R.H. (2015). In the right place at the right time: visualizing and understanding mRNA localization. Nat Rev Mol Cell Biol *16*, 95-109.

Campbell, P.D., Chao, J.A., Singer, R.H., and Marlow, F.L. (2015). Dynamic visualization of transcription and RNA subcellular localization in zebrafish. Development *142*, 1368-1374.

Chin, A., and Lecuyer, E. (2017). RNA localization: Making its way to the center stage. Biochim Biophys Acta *1861*, 2956-2970.

Costa, G., Harrington, K.I., Lovegrove, H.E., Page, D.J., Chakravartula, S., Bentley, K., and Herbert, S.P. (2016). Asymmetric division coordinates collective cell migration in angiogenesis. Nat Cell Biol *18*, 1292-1301.

De Bock, K., Georgiadou, M., Schoors, S., Kuchnio, A., Wong, B.W., Cantelmo, A.R., Quaegebeur, A., Ghesquiere, B., Cauwenberghs, S., Eelen, G., *et al.* (2013). Role of PFKFB3-driven glycolysis in vessel sprouting. Cell *154*, 651-663.

Fusco, D., Accornero, N., Lavoie, B., Shenoy, S.M., Blanchard, J.M., Singer, R.H., and Bertrand, E. (2003). Single mRNA molecules demonstrate probabilistic movement in living mammalian cells. Curr Biol *13*, 161-167.

Gerhardt, H., Golding, M., Fruttiger, M., Ruhrberg, C., Lundkvist, A., Abramsson, A., Jeltsch, M., Mitchell, C., Alitalo, K., Shima, D., *et al.* (2003). VEGF guides angiogenic sprouting utilizing endothelial tip cell filopodia. J Cell Biol *161*, 1163-1177.

Harris, E.S., and Nelson, W.J. (2010). Adenomatous polyposis coli regulates endothelial cell migration independent of roles in beta-catenin signaling and cell-cell adhesion. Mol Biol Cell *21*, 2611-2623.

Herbert, S.P., and Stainier, D.Y. (2011). Molecular control of endothelial cell behaviour during blood vessel morphogenesis. Nat Rev Mol Cell Biol *12*, 551-564.

Hogan, B.M., and Schulte-Merker, S. (2017). How to Plumb a Pisces: Understanding Vascular Development and Disease Using Zebrafish Embryos. Dev Cell *42*, 567-583.

Ioannou, M.S., Bell, E.S., Girard, M., Chaineau, M., Hamlin, J.N., Daubaras, M., Monast, A., Park, M., Hodgson, L., and McPherson, P.S. (2015). DENND2B activates Rab13 at the leading edge of migrating cells and promotes metastatic behavior. J Cell Biol *208*, 629-648.

Isogai, S., Lawson, N.D., Torrealday, S., Horiguchi, M., and Weinstein, B.M. (2003). Angiogenic network formation in the developing vertebrate trunk. Development *130*, 5281-5290.

Jakobsen, K.R., Sorensen, E., Brondum, K.K., Daugaard, T.F., Thomsen, R., and Nielsen, A.L. (2013). Direct RNA sequencing mediated identification of mRNA localized in protrusions of human MDA-MB-231 metastatic breast cancer cells. J Mol Signal *8*, 9.

Jin, S.W., Beis, D., Mitchell, T., Chen, J.N., and Stainier, D.Y. (2005). Cellular and molecular analyses of vascular tube and lumen formation in zebrafish. Development *132*, 5199-5209.

Kislauskis, E.H., Zhu, X., and Singer, R.H. (1994). Sequences responsible for intracellular localization of beta-actin messenger RNA also affect cell phenotype. J Cell Biol *127*, 441-451.

Kislauskis, E.H., Zhu, X., and Singer, R.H. (1997). beta-Actin messenger RNA localization and protein synthesis augment cell motility. J Cell Biol *136*, 1263-1270.

Krause, M., and Gautreau, A. (2014). Steering cell migration: lamellipodium dynamics and the regulation of directional persistence. Nat Rev Mol Cell Biol *15*, 577-590.

Lee, I.Y., Kim, J., Ko, E.M., Jeoung, E.J., Kwon, Y.G., and Choe, J. (2002). Interleukin-4 inhibits the vascular endothelial growth factor- and basic fibroblast growth factor-induced angiogenesis in vitro. Mol Cells *14*, 115-121.

Liang, C.C., Park, A.Y., and Guan, J.L. (2007). In vitro scratch assay: a convenient and inexpensive method for analysis of cell migration in vitro. Nat Protoc *2*, 329-333.

Liao, G., Simone, B., and Liu, G. (2011). Mis-localization of Arp2 mRNA impairs persistence of directional cell migration. Exp Cell Res *317*, 812-822.

Mardakheh, F.K., Paul, A., Kumper, S., Sadok, A., Paterson, H., McCarthy, A., Yuan, Y., and Marshall, C.J. (2015). Global Analysis of mRNA, Translation, and Protein Localization: Local Translation Is a Key Regulator of Cell Protrusions. Dev Cell *35*, 344-357.

Marzesco, A.M., Dunia, I., Pandjaitan, R., Recouvreur, M., Dauzonne, D., Benedetti, E.L., Louvard, D., and Zahraoui, A. (2002). The small GTPase Rab13 regulates assembly of functional tight junctions in epithelial cells. Mol Biol Cell *13*, 1819-1831.

Mayor, R., and Etienne-Manneville, S. (2016). The front and rear of collective cell migration. Nat Rev Mol Cell Biol *17*, 97-109.

Mili, S., Moissoglu, K., and Macara, I.G. (2008). Genome-wide screen reveals APC-associated RNAs enriched in cell protrusions. Nature *453*, 115-119.

Miller, S., Yasuda, M., Coats, J.K., Jones, Y., Martone, M.E., and Mayford, M. (2002). Disruption of dendritic translation of CaMKIIalpha impairs stabilization of synaptic plasticity and memory consolidation. Neuron *36*, 507-519.

Moreno-Mateos, M.A., Vejnar, C.E., Beaudoin, J.D., Fernandez, J.P., Mis, E.K., Khokha, M.K., and Giraldez, A.J. (2015). CRISPRscan: designing highly efficient sgRNAs for CRISPR-Cas9 targeting in vivo. Nat Methods *12*, 982-988.

Nakatsu, M.N., and Hughes, C.C. (2008). An optimized three-dimensional in vitro model for the analysis of angiogenesis. Methods Enzymol *443*, 65-82.

Park, H.Y., Lim, H., Yoon, Y.J., Follenzi, A., Nwokafor, C., Lopez-Jones, M., Meng, X., and Singer, R.H. (2014). Visualization of dynamics of single endogenous mRNA labeled in live mouse. Science *343*, 422-424.

Park, H.Y., Trcek, T., Wells, A.L., Chao, J.A., and Singer, R.H. (2012). An unbiased analysis method to quantify mRNA localization reveals its correlation with cell motility. Cell Rep *1*, 179-184.

Pfeffer, S.R., Dirac-Svejstrup, A.B., and Soldati, T. (1995). Rab GDP dissociation inhibitor: putting rab GTPases in the right place. J Biol Chem *270*, 17057-17059.

Ruhrberg, C., Gerhardt, H., Golding, M., Watson, R., Ioannidou, S., Fujisawa, H., Betsholtz, C., and Shima, D.T. (2002). Spatially restricted patterning cues provided by heparin-binding VEGF-A control blood vessel branching morphogenesis. Genes Dev *16*, 2684-2698.

Sakane, A., Abdallah, A.A., Nakano, K., Honda, K., Ikeda, W., Nishikawa, Y., Matsumoto, M., Matsushita, N., Kitamura, T., and Sasaki, T. (2012). Rab13 small G protein and junctional Rab13-binding protein (JRAB) orchestrate actin cytoskeletal organization during epithelial junctional development. J Biol Chem *287*, 42455-42468.

Sakane, A., Alamir Mahmoud Abdallah, A., Nakano, K., Honda, K., Kitamura, T., Imoto, I., Matsushita, N., and Sasaki, T. (2013). Junctional Rab13-binding protein (JRAB) regulates cell spreading via filamins. Genes Cells *18*, 810-822.

Schedlich, L., Hill, M., and Lockett, T. (1997). Antisense inhibition of beta-actin mRNA localization and its effect on smooth muscle cell migration. Biol Cell *89*, 113-122.

Seabra, M.C., Mules, E.H., and Hume, A.N. (2002). Rab GTPases, intracellular traffic and disease. Trends Mol Med *8*, 23-30.

Shen, F., and Seabra, M.C. (1996). Mechanism of digeranylgeranylation of Rab proteins. Formation of a complex between monogeranylgeranyl-Rab and Rab escort protein. J Biol Chem *271*, 3692-3698.

Shestakova, E.A., Singer, R.H., and Condeelis, J. (2001). The physiological significance of beta - actin mRNA localization in determining cell polarity and directional motility. Proc Natl Acad Sci U S A *98*, 7045-7050.

Stuart, H.C., Jia, Z., Messenberg, A., Joshi, B., Underhill, T.M., Moukhles, H., and Nabi, I.R. (2008). Localized Rho GTPase activation regulates RNA dynamics and compartmentalization in tumor cell protrusions. J Biol Chem *283*, 34785-34795.

tom Dieck, S., Kochen, L., Hanus, C., Heumuller, M., Bartnik, I., Nassim-Assir, B., Merk, K., Mosler, T., Garg, S., Bunse, S.*, et al.* (2015). Direct visualization of newly synthesized target proteins in situ. Nat Methods *12*, 411-414.

Villefranc, J.A., Amigo, J., and Lawson, N.D. (2007). Gateway compatible vectors for analysis of gene function in the zebrafish. Dev Dyn *236*, 3077-3087.

Wang, T., Hamilla, S., Cam, M., Aranda-Espinoza, H., and Mili, S. (2017). Extracellular matrix stiffness and cell contractility control RNA localization to promote cell migration. Nat Commun *8*, 896.

Wu, C., Agrawal, S., Vasanji, A., Drazba, J., Sarkaria, S., Xie, J., Welch, C.M., Liu, M., Anand-Apte, B., and Horowitz, A. (2011). Rab13-dependent trafficking of RhoA is required for directional migration and angiogenesis. J Biol Chem *286*, 23511-23520.

Wu, K.Y., Hengst, U., Cox, L.J., Macosko, E.Z., Jeromin, A., Urquhart, E.R., and Jaffrey, S.R. (2005). Local translation of RhoA regulates growth cone collapse. Nature *436*, 1020-1024.

Zahraoui, A., Joberty, G., Arpin, M., Fontaine, J.J., Hellio, R., Tavitian, A., and Louvard, D. (1994). A small rab GTPase is distributed in cytoplasmic vesicles in non polarized cells but colocalizes with the tight junction marker ZO-1 in polarized epithelial cells. J Cell Biol *124*, 101-115.

Zappulo, A., van den Bruck, D., Ciolli Mattioli, C., Franke, V., Imami, K., McShane, E., Moreno-Estelles, M., Calviello, L., Filipchyk, A., Peguero-Sanchez, E.*, et al.* (2017). RNA localization is a key determinant of neurite-enriched proteome. Nat Commun *8*, 583.

FIGURE LEGENDS

Figure 1. *RAB13* mRNA is localized to protrusions in endothelial cells during migration.

(A) Scheme depicts the Transwell culture strategy. HUVECs cultured in the upper chamber extend protrusions through the Transwell membrane pores into the lower chamber containing VEGF-A.

(B) RNA-seq data are plotted in reads per kilobase of transcripts per million reads (RPKM) against fold change (FC) levels of protrusions over cell bodies; light-grey data are transcripts with low expression and not considered; data are mean values represented in $\log_2$ (n=2 replicates).

(C) Bar graph representing qPCR analysis of mRNA enrichment in protrusions; data are mean±s.d. (n=3 replicates).

(D) smFISH detection of *RAB13* and *GAPDH* mRNA in an exemplar HUVEC; scale bar: 20 µm.

(E) Scatter plot shows the Polarization Index of *GAPDH* and *RAB13* mRNA detected by smFISH in single HUVECs; lines are mean values (n=33 cells).

(F) smFISH analysis of *RAB13* and *GAPDH* mRNA distribution in an exemplar tip cell within a fibrin sprout; scale bar: 20 µm.

(G) Scatter plot represents the relative distance of *GAPDH* and *RAB13* mRNA center of distribution to the nucleus in individual tip cells; lines are mean values (n=38 cells).

See also **Figure S1.**

Figure 2. *RAB13* mRNA is translated in endothelial cell protrusions.

(A) Scheme depicts the strategy to label newly synthesized proteins in HUVEC protrusions formed in Tanswell cultures.

(B) Immunofluorescence detection of Puromycin incorporation into HUVEC protrusions present in the lower Transwell membrane side (representative of 3 replicates); scale bar: 10 µm.

(C) Puro-PLA analysis of newly synthesized RAB13 in HUVEC protrusions present in the lower Transwell membrane side (representative of 3 replicates); scale bar: 10 µm.

(D) Scatter plot shows the quantification of RAB13 Puro-PLA puncta number normalized to protrusion area; lines are mean values (n≥44 protrusions).

See also **Figure S2.**

Figure 3. The 3' UTR of *rab13* localizes transcripts to endothelial cell protrusions *in vivo*.

(A) bEnd.3 cells co-transfected with plasmids expressing Lyn-mCherry, MCP-GFPnls and 24xMS2-*RAB13* 3'UTR or 24xMS2- empty (representative of 21 cells); arrow: non-nuclear localization of MCP-GFPnls; scale bars: 20 µm.

(B) Bar graph represents the percentage of bEND.3 cells with MCP-GFP localized to protrusions when co-transfected with deletion versions of *RAB13* 3'UTR tagged with 24x MS2 hairpins; data are mean±s.d. (n≥30 cells).

(C) smFISH analysis of representative Wt and Δ91-280 *RAB13* 3'UTR HUVECs; arrow: accumulation of *RAB13* transcripts in a protrusion; scale bar: 20 µm.

(D) Scatter plot shows the Polarization Index of *GAPDH* and *RAB13* mRNA detected by smFISH in Wt and Δ91-280 *RAB13* 3'UTR HUVECs; lines are mean values (n=10 cells); n.s. – non-significant.

(E) Representative time-lapse confocal micrographs of an ISV sprouting cell in a *Tg(fli1ep:*MCP-GFPnls*)* 28 hpf zebrafish embryo (time point 0 min); embryo injected at one-cell stage with *rab13* 3'UTR tagged with Lyn-mCherry and 24x MS2 hairpins; arrows: non-nuclear localization of MCP-GFPnls; scale bars: 20 µm. See also **Movie S1** and **Figure S3.**

Figure 4. *RAB13* mRNA localization regulates protrusion formation in angiogenesis *in-vivo*.

(A) smFISH analysis of representative cultured cells derived from wild type (+/+) and homozygous (-/-) Δ482 *rab13* 3' UTR embryos; arrows: *rab13* mRNA; scale bar: 10 µm.

(B) Scatter plot shows the Polarization Index of *rab13* mRNA detected by smFISH in individual Δ482 *rab13* 3' UTR zebrafish cells; lines are mean values (n≥33 cells each genotype).

(C) Time-lapse confocal micrographs of representative +/+ and -/- Δ482 *rab13* 3' UTR embryos starting at 25 hpf (time point 0 min); arrows: extra branches emerging from the main ISVs; DLAV– dorsal longitudinal anastomotic vessel, HM – horizontal myoseptum; scale bars: 50 µm. See also **Movie S2.**

(D) Schematic diagram representing the two most common types of branching observed in ISVs of zebrafish embryos.

(E) Bar graph shows the frequency of extra branching occurring at the horizontal myoseptum in Δ482 *rab13* 3' UTR zebrafish embryos; data are mean±s.d. (n≥7 embryos each genotype). See also **Figure S4.**

Figure 1

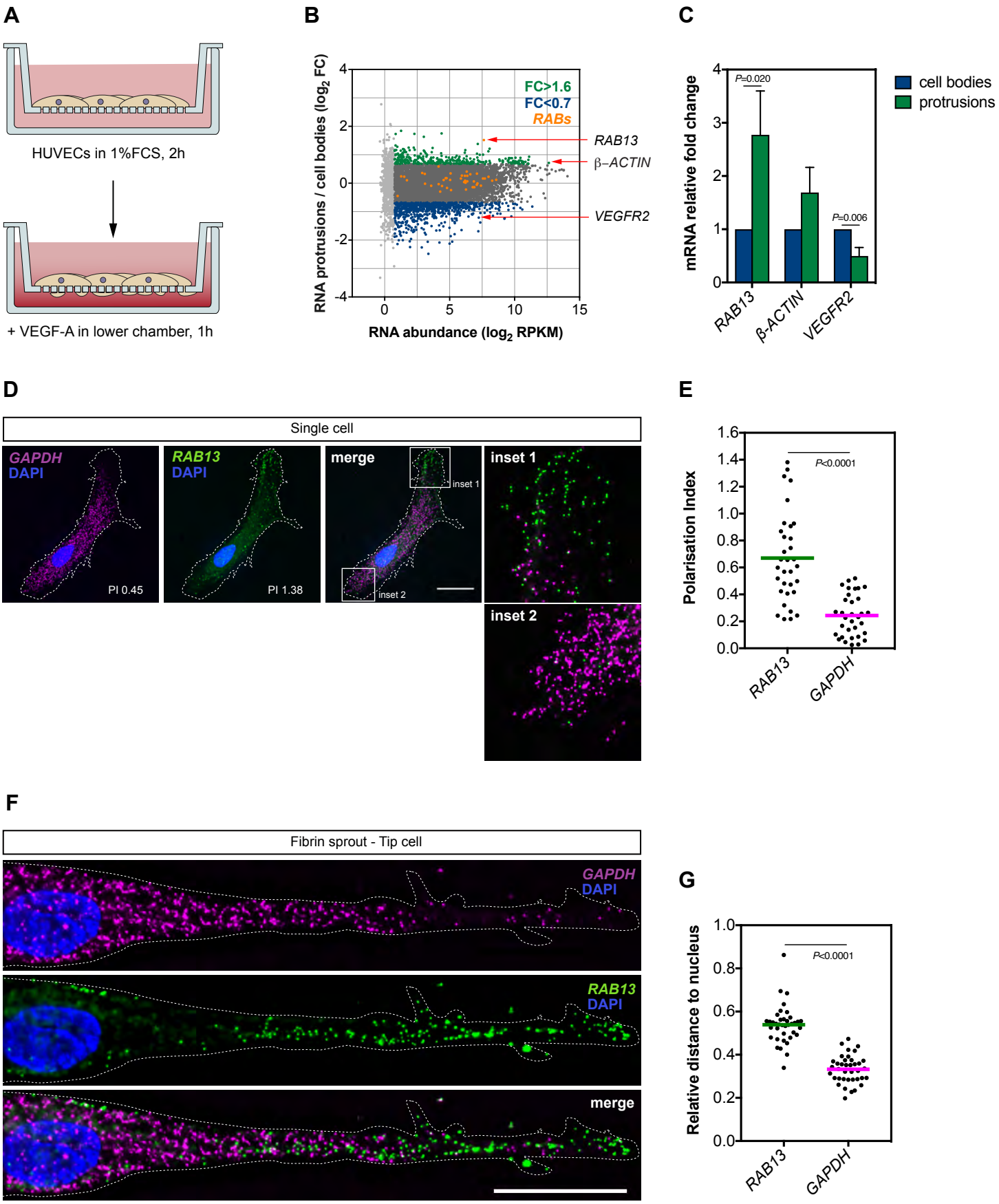
A
HUVECs in 1%FCS, 2h
+ VEGF-A in lower chamber, 1h
B
FC>1.6
FC<0.7
RABs
RAB13
β–ACTIN
VEGFR2
RNA protrusions / cell bodies (log2 FC)
RNA abundance (log2 RPKM)
C
P=0.020
P=0.006
cell bodies
protrusions
mRNA relative fold change
RAB13
β-ACTIN
VEGFR2
D
Single cell
GAPDH
DAPI
PI 0.45
RAB13
DAPI
PI 1.38
merge
inset 1
inset 2
E
P<0.0001
Polarisation Index
RAB13
GAPDH
F
Fibrin sprout - Tip cell
GAPDH
DAPI
RAB13
DAPI
merge
G
P<0.0001
Relative distance to nucleus
RAB13
GAPDH

Figure 2

A

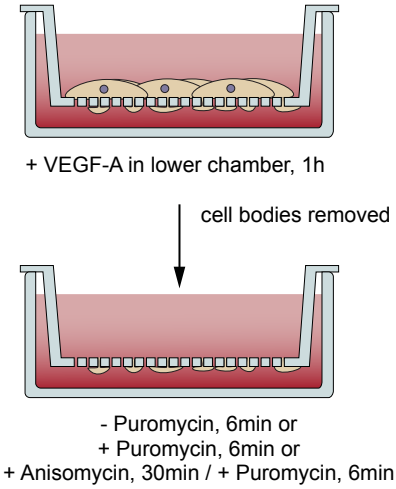

B

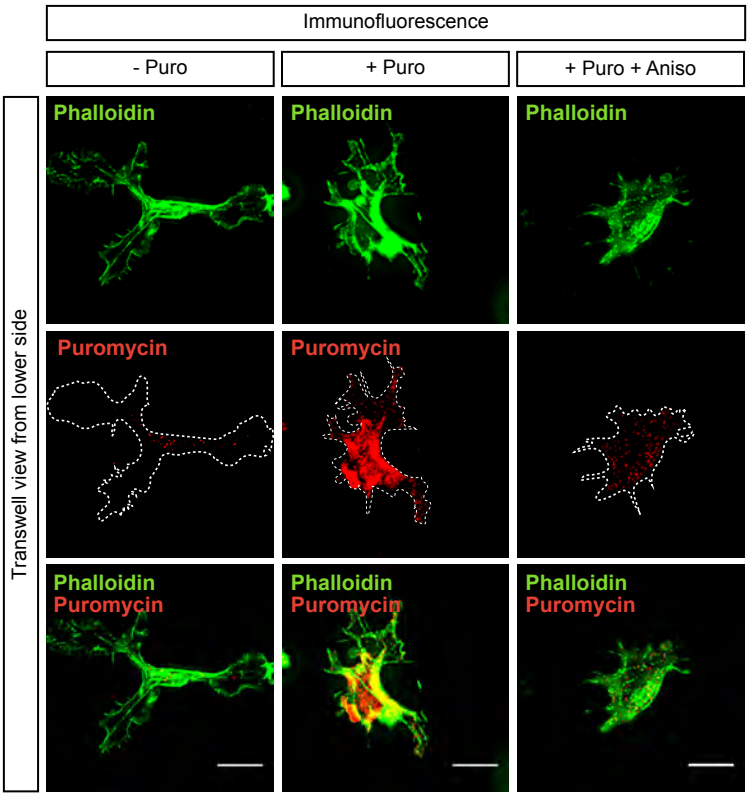

C

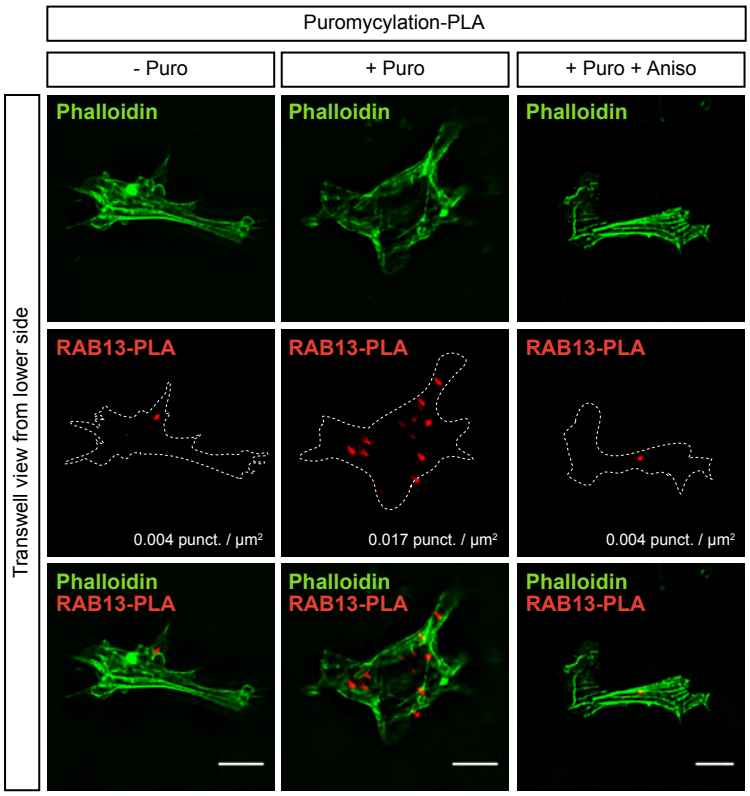

D

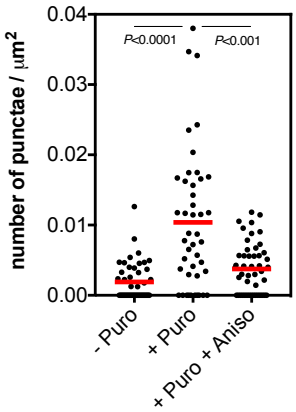

Figure 3

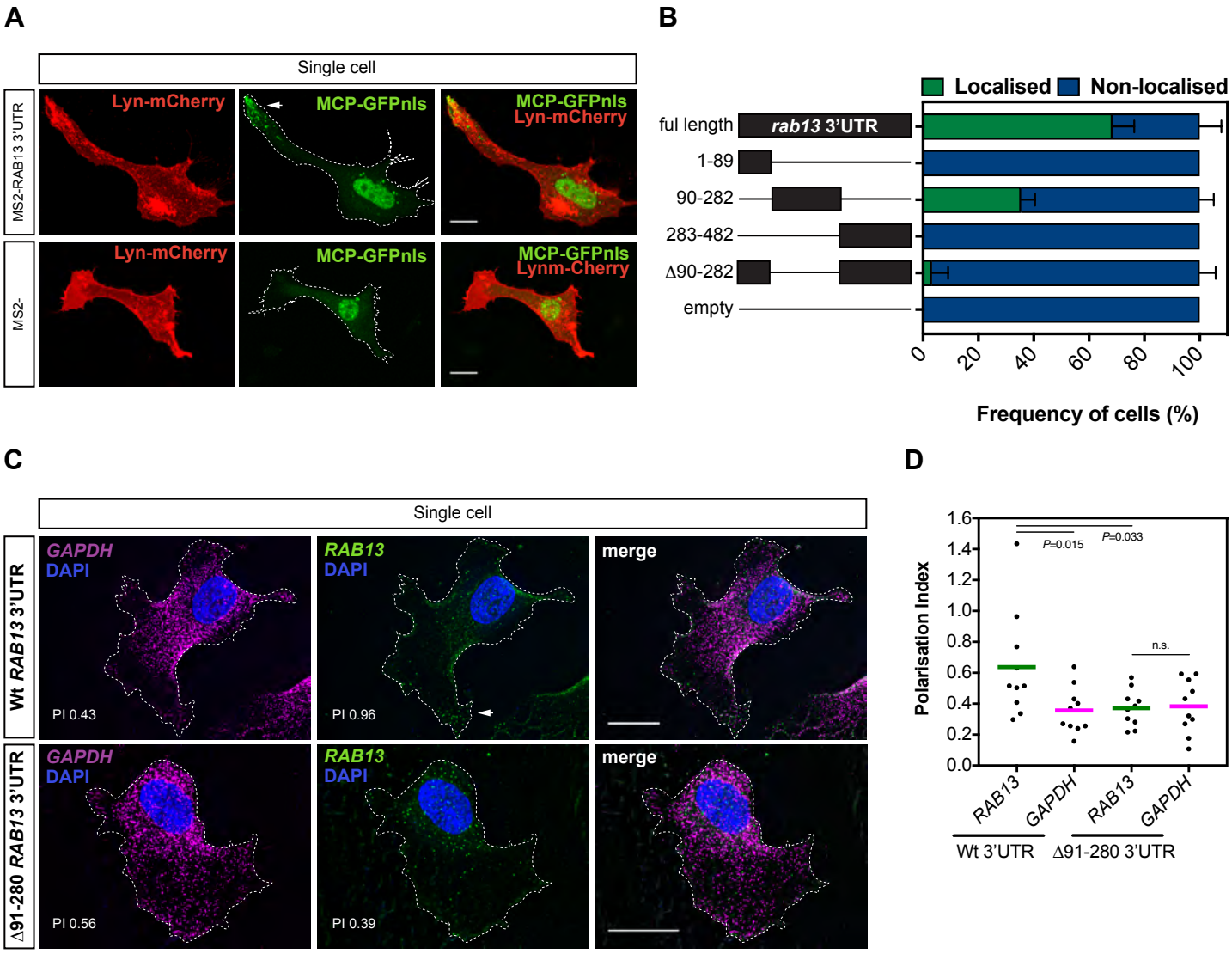
A
Single cell
MS2-RAB13 3'UTR
MS2-
Lyn-mCherry
MCP-GFPnls
MCP-GFPnls
Lyn-mCherry
Lyn-mCherry
MCP-GFPnls
MCP-GFPnls
Lynm-Cherry
B
Localised
Non-localised
ful length
rab13 3'UTR
1-89
90-282
283-482
Δ90-282
empty
0
20
40
60
80
100
Frequency of cells (%)
C
Single cell
Wt RAB13 3'UTR
Δ91-280 RAB13 3'UTR
GAPDH
DAPI
RAB13
DAPI
merge
PI 0.43
PI 0.96
PI 0.56
PI 0.39
D
Polarisation Index
1.6
1.4
1.2
1.0
0.8
0.6
0.4
0.2
0.0
P=0.015
P=0.033
n.s.
RAB13
GAPDH
RAB13
GAPDH
Wt 3'UTR
Δ91-280 3'UTR
E
ISV sprouting cell
Lyn-mCherry
MCP-GFPnls
MCP-GFPnls
Lyn-mCherry
T0 + 30 min
T0 + 60 min
T0 + 90 min
inset

Figure 4

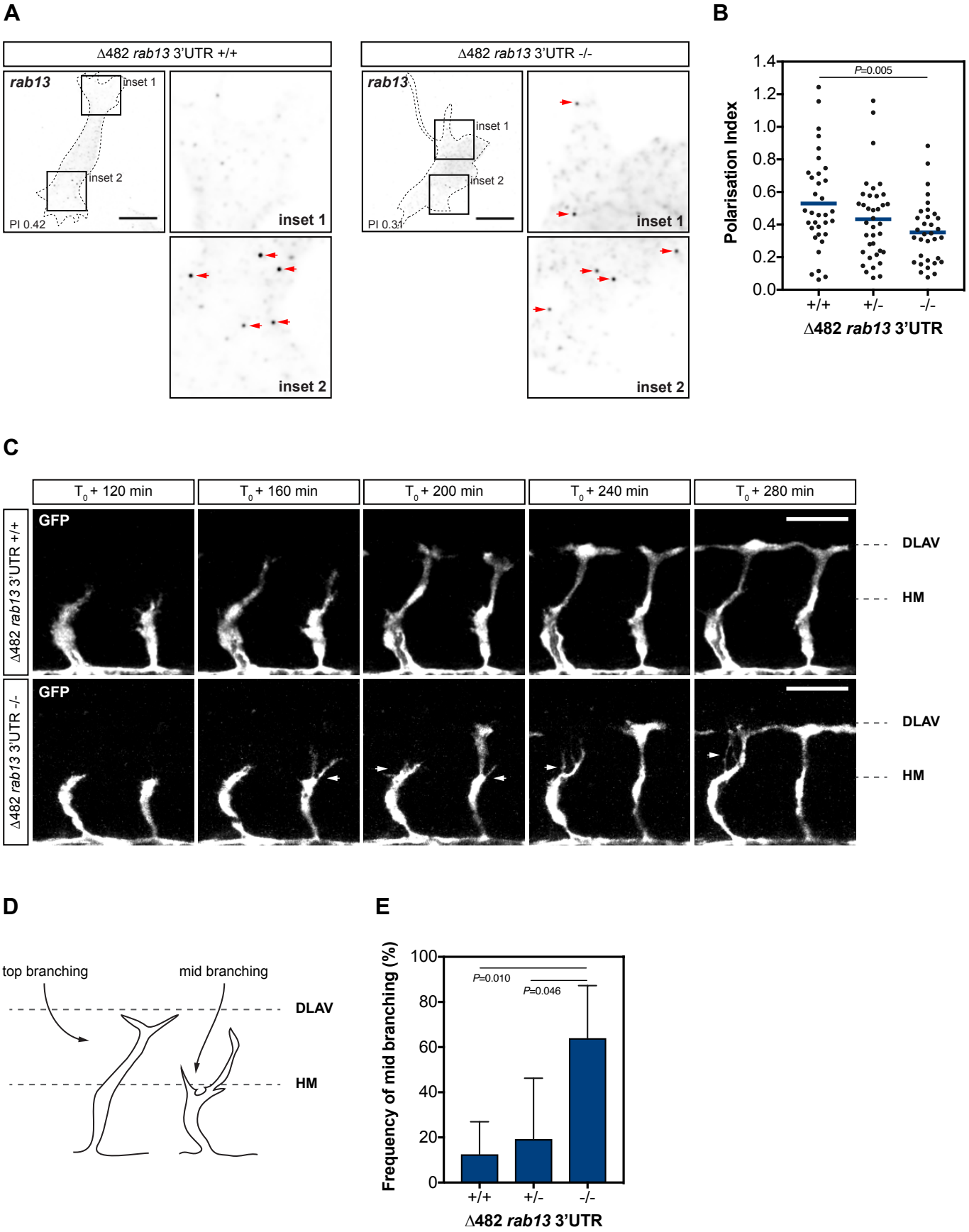
A
Δ482 rab13 3'UTR +/+
rab13
inset 1
inset 2
PI 0.42
inset 1
inset 2
Δ482 rab13 3'UTR -/-
rab13
inset 1
inset 2
PI 0.31
inset 1
inset 2
B
P=0.005
Polarisation Index
1.4
1.2
1.0
0.8
0.6
0.4
0.2
0.0
+/+
+/-
-/-
Δ482 rab13 3'UTR
C
T0 + 120 min
T0 + 160 min
T0 + 200 min
T0 + 240 min
T0 + 280 min
Δ482 rab13 3'UTR +/+
Δ482 rab13 3'UTR -/-
GFP
DLAV
HM
D
top branching
mid branching
DLAV
HM
E
P=0.010
P=0.046
Frequency of mid branching (%)
100
80
60
40
20
0
+/+
+/-
-/-
Δ482 rab13 3'UTR